Light-induced modification of *a*-SiO_x II: Laser crystallization

Andreas Janotta,[a] Yavuz Dikce, Matthias Schmidt, Christopher Eisele, and Martin Stutzmann
Walter Schottky Institut, Technische Universität München, Am Coulombwall 3, 85748 Garching, Germany

Martina Luysberg and Lothar Houben
Forschungszentrum Jülich, IFF, 52425 Jülich, Germany

(Received 12 August 2003; accepted 14 January 2004)

Amorphous hydrogenated silicon suboxides (*a*-SiO_x:H) were deposited by plasma enhanced chemical vapor deposition from the source gases SiH_4, H_2, and CO_2. The band gap of the samples can be tuned from 1.9 to 3.0 eV by varying the oxygen content from 0 to 50 at. %. H-effused samples were irradiated by ultraviolet laser pulses with intensities up to 480 mJ/cm^2. The structural changes and the crystallization behavior were investigated as a function of oxygen content and laser intensity. A decrease of the melting threshold by a factor of two with increasing oxygen content (0–44 at. %) was observed for the SiO_x samples. Above the respective melting thresholds, not only a deterioration of the structural properties but also indications of a segregation of Si crystallites were found. Raman spectroscopy and transmission electron microscopy gave evidence for the existence of Si crystallites up to oxygen contents of 40 at. %. The crystal size reached an optimum for oxygen concentrations between 10 and 30 at. %. © *2004 American Institute of Physics.*
[DOI: 10.1063/1.1667008]

I. INTRODUCTION

The effects of intensive illumination generally are detrimental for the properties of amorphous or glassy semiconductors as a result of light-induced degradation effects.[1–8] However, under certain circumstances strong irradiation can also help to modify and enhance the material quality in a desired way. In the case of amorphous silicon, if the intensity of the incident light is strong enough to melt the amorphous film (partly or completely), it can form (poly-)crystalline material upon solidification. As a result of the increase of crystallinity the electrical conductivity of the films improves drastically. Amorphous, nano-, or microcrystalline layers deposited at relatively low cost on various substrates (quartz, glass, plastic, etc.) are favorable starting materials for a subsequent crystallization by laser light. For amorphous silicon (*a*-Si), which has been most extensively studied, it was observed that laser crystallization is less successful when the crystal size is too small and many grain boundaries prevent an efficient electric transport. Furthermore, illumination by continuous wave lasers turned out to cause an unwanted diffusion of substrate contaminants into the film.[9,10] Therefore, short laser pulses which leave the substrate unaffected are used to crystallize *a*-Si.[11–17] In this case, however, hydrogen-effused samples are required or the hydrogen atoms have to be effused at temperatures above 300 °C. This is necessary to avoid an explosive hydrogen effusion which would damage the samples during pulsed laser processing.

Many aspects have to be taken into account to achieve the advantageous growth of large crystals by means of pulsed lasers. It was found that grain sizes considerably larger than the sample thickness can form only in a narrow process window where the film is nearly completely melted. Then, only a few solid islands remain in the liquid silicon and form nucleation centers at sufficiently large distances so that extended crystals can develop. This regime was called superlateral growth (SLG) by Im *et al.*[11] However, the SLG is very sensitive to parameters such as the film thickness, the laser intensity, the beam profile, or the thermal conductivity of the substrate and therefore difficult to stabilize. At lower laser energy densities, too many nucleation seeds remain in the partially melted film and only lead to small crystal grains. The same is true for a complete melting of the *a*-Si layer. Then, numerous nucleation sites form statistically in the supercooled melt and limit the grain size. In order to control the grain boundaries and grain size it is favorable to fully melt the film only in selected areas, whereas the adjacent regions, from where the lateral crystal growth starts, are only partially liquified. This area selection can be realized by antireflection coatings,[12] beam shaping (masks, or holographic techniques),[12,16,17] or laser interference.[14,15,17] Sequential scanning of the beam profile over the film in distances slightly smaller than the typical lateral grain size allows one to extend the area of the desired large crystal growth by using the already existing grains as starting points for further nucleation.

Although the laser crystallization of amorphous silicon has been investigated in detail, not much insight exists for amorphous alloys of silicon with elements such as oxygen, carbon, or nitrogen. In this article, we focus on the laser irradiation and crystallization behavior of amorphous silicon suboxides (*a*-SiO_x). By varying the oxygen content [O] between 0 and 50 at. % the material properties can be gradually tuned from an amorphous overconstrained semiconductor (with an average coordination close to a value of four) to-

[a]Author to whom correspondence should be addressed; electronic mail: janotta@wsi.tum.de

wards a semiconducting glass (which exhibits a glass transition and is more flexible due to the lack of topological constraints).[1] Thus, a systematic study of laser crystallization as a function of the oxygen concentration can be performed.

II. EXPERIMENTAL DETAILS

Hydrogenated amorphous silicon suboxides (a-SiO_x:H) were deposited by plasma enhanced chemical vapor deposition from the source gases SiH_4, H_2 and CO_2.[18] By varying the SiH_4/CO_2 gas flow ratio, oxygen concentrations between 0 and 50 at. % can be achieved with a residual carbon contamination below 1 at. %. The respective hydrogen concentrations were between 15 and 25 at. %. This leads to optical gaps (E_{04}, the energy where the absorption coefficient reaches $10^4\,cm^{-1}$) between 1.9 and 3.0 eV. The intrinsic silicon suboxide films examined in this study (thickness 500–1000 nm) were deposited on quartz and Corning 7059 glass substrates at 250 °C. The oxygen concentrations were varied between 0 and 44 at. % and were determined by energy dispersive x-ray spectroscopy which was calibrated by quantitative elastic recoil detection analysis. All oxygen contents given in the text refer to the atomic ratio [O]/([O]+[Si]).

For laser crystallization, a major fraction of the hydrogen in the samples had to be removed to avoid explosive effusion of hydrogen during the laser pulse. The H effusion was performed under N_2 atmosphere at temperatures of 450 °C for 1 h, thus avoiding crystallization. Single (in some cases also multiple) pulses of a frequency-tripled Nd:YAG laser (8 ns, 355 nm) were applied to crystallize the H-effused a-SiO_x samples (0–44 at. %). The beam diameter was roughly 8 mm and the pulse energy densities were varied between 0 and 480 mJ/cm^2. Laser irradiation was performed in air and at room temperature. Homogeneous illumination as well as two-beam interference were used for crystallization, the latter leading to a structuring of the samples in the form of a line grating. The surface melting threshold of the SiO_x samples with different oxygen concentrations was determined by measurements of the transient reflectance during laser irradiation, using a HeNe laser as a probe beam and fast photodiodes for detection. The modifications resulting from the pulsed crystallization were investigated by means of the absorption spectra of the samples as a function of laser pulse energy density and oxygen content. The absorption coefficient α, the optical gap E_{04}, the Urbach energy E_0, and the subgap defect absorption were determined from photothermal deflection spectroscopy[19] and optical transmission measurements. The interference-crystallized samples were also analyzed by means of atomic force microscopy (AFM). The crystallinity and crystal quality of the laser crystallized SiO_x samples were investigated by room temperature Raman spectroscopy for the different pulse energies and oxygen concentrations. The Raman signal was excited by an argon ion laser (λ=488 nm), resolved by a triple monochromator and detected by a charge coupled device camera cooled with liquid N_2. Also, bright and dark field images as well as diffraction patterns of the laser irradiated samples, prepared in cross section geometry, were recorded by means of transmission electron microscopy (TEM).

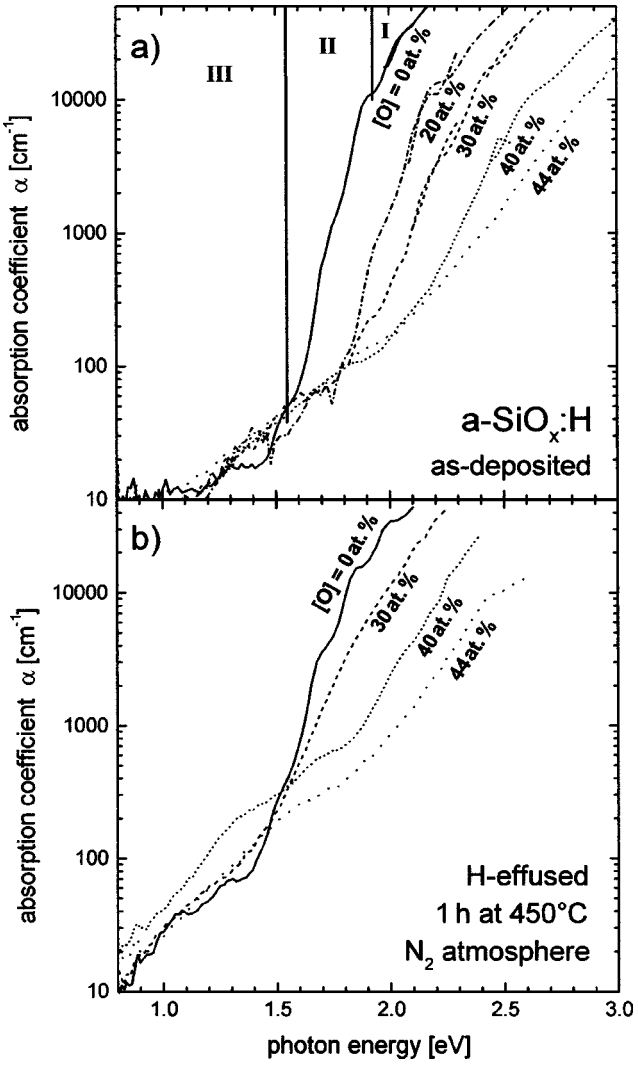

FIG. 1. Absorption spectra of as-deposited (a) and H-effused (b) intrinsic a-SiO_x:H with oxygen contents between 0 and 44 at. %. In the upper graph, the spectral regions of band-to-band (I), band tail (II), and of defect absorption (III) are indicated for the sample without oxygen (a-Si:H).

III. OPTICAL PROPERTIES OF a-SiO_x

The properties of amorphous silicon suboxides such as the optical gap, the Urbach tail, or the defect density strongly depend on the concentration of oxygen and, to a minor extent, also on the amount of hydrogen which is present in the samples. The hydrogen effusion of the samples leads to additional changes of these parameters. The absorption coefficient α allows us to monitor compositional and structural changes of SiO_x samples.

Figure 1(a) shows the absorption spectra for a set of as-deposited, intrinsic a-SiO_x:H ([O]=0–44 at. %) which elucidate the changes in the electronic density of states with increasing oxygen content. For the a-Si:H sample (0 at. % [O]), the three characteristic regions of absorption are indicated. Region I corresponds to band-to-band absorption, region II originates from absorption processes involving band tail states, and region III arises from absorption via dangling

bond defect states in the middle of the forbidden gap [known from electron paramagnetic resonance measurements]. These regions are also discernible for the other curves, however, become less distinguishable with rising oxygen concentration. The value of the band gap E_{04} increases from approximately 1.9 to 2.8 eV for [O] between 0 and 44 at. %. The band tails (II) of our SiO_x samples start out with an Urbach energy of about 70 meV for *a*-Si:H and broaden significantly with rising oxygen content. Thus, the presence of oxygen increases the disorder in the amorphous films. Also the subgap absorption via defect states changes as a function of the oxygen content. With increasing [O] the spectral region of defect absorption broadens significantly. Correspondingly, the overall number of dangling bonds is roughly 1 order of magnitude higher for the largest oxygen concentrations (44 at. %) compared to pure amorphous silicon. Note, that our samples with [O]=0 at. % have higher Urbach energies and a larger subgap defect absorption than optimized state-of-the-art *a*-Si:H samples because of a residual oxygen contamination and nonoptimized deposition conditions.

The influence of the hydrogen effusion procedure (1 h at 450 °C) on the SiO_x absorption spectra is shown in part (b) of Fig. 1. After a major part of the H atoms has left the sample, the value of the optical gap E_{04} is smaller for all samples. For *a*-Si:H, the presence of H results in the formation of Si–H states in the valence band which replace Si–Si states at the valence band edge and thus widen the gap.[20–25] On the other hand, an outdiffusion of H reverses this process and consequently reduces E_{04}.[8,20,26,27] In the case of silicon suboxides it can be assumed that similar processes lead to a comparable relative change of E_{04}.[18] The fact that the decrease of the optical gap is more pronounced for samples with higher [O] can be understood by their larger initial hydrogen concentration. In addition, a broadening of the Urbach tails and a rise of the subgap absorption are observed, which indicate that both the structural disorder and the dangling bond concentration are increased as a consequence of the hydrogen loss. Therefore, the H-effused samples required for laser crystallization not only possess smaller band gaps, but also higher disorder and defect densities. However, this reduction of structural quality is not a real disadvantage, since the effects of pulsed laser irradiation have a much larger influence on the resulting sample structure than the effusion of hydrogen.

IV. LASER CRYSTALLIZATION

A. Surface melting threshold

In order to compare the crystallization behavior of silicon suboxides with different oxygen contents, in a first step the surface melting threshold of the samples as a function of [O] was determined by transient reflectance measurements. If the incident laser pulse is intense enough to melt the film surface, a significant increase of the reflectivity of the liquified material can be observed. Thus, the intensity of a reflected HeNe laser probe beam displays a transient peak which can be used to monitor the melting and solidification process of the sample surface. Figure 2 shows the transient changes in the reflectivity of four *a*-SiO_x samples with 0, 20, 30, and 40 at. % [O] for increasing pulse energy densities I_L. The irradiation was performed with a frequency-tripled Nd:YAG laser at 355 nm (≈3.5 eV), which corresponds to a photon energy above the optical band gap of all investigated samples. The time slot of the 8 ns laser pulse is indicated by an arrow in each figure. For all oxygen concentrations a transient peak in the curves, corresponding to the melted state, can be recognized above a certain threshold energy density I_{thr}. When the *a*-Si sample [Fig. 2(a)] is irradiated by pulse energy densities up to 70 mJ/cm^2 (at $t \approx 120$ ns on the given time scale), only a slight decrease of the signal due to sample heating is visible. Above $I_{thr} \approx 80$ mJ/cm^2, a peak in the reflectivity appears which increases in intensity and duration. For pulse energy densities of 150 mJ/cm^2 (i.e., twice the melting threshold of *a*-Si) the liquified state persists for almost 50 ns after the laser irradiation. With rising [O], the SiO_x samples [Figs. 2(b)–2(d)] exhibit similar behavior, however, the melting threshold values are significantly reduced. For the sample with 20 at. % oxygen [Fig. 2(b)], I_{thr} is still between 60 and 70 mJ/cm^2. For the films with larger [O] [Figs. 2(c)–2(d)], the limit for melting is reduced to around 40 mJ/cm^2. Also, the transient reflectance signal tends to become weaker for suboxides with higher oxygen contents since phase separation occurs (see below) and the molten Si/SiO_2 mixture does not exhibit such a pronounced metallic character as pure liquid silicon.

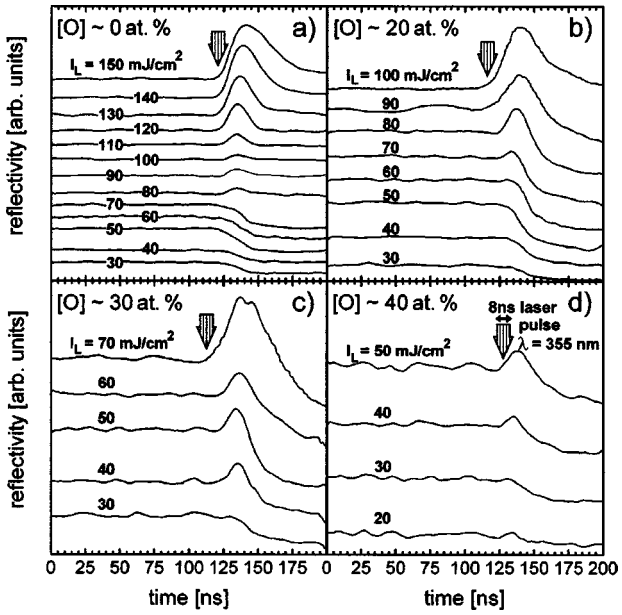

FIG. 2. Transient reflectivity of *a*-SiO_x samples with 0, 20, 30, and 40 at. % oxygen. The samples were irradiated with 8 ns Nd:YAG laser pulses (λ =355 nm) at different laser energy densities I_L between 20 and 150 mJ/cm^2. The time and duration of the laser pulses are indicated by arrows. A HeNe laser at 632 nm was used as a probe laser.

Figure 3 summarizes the dependence of the SiO_x melting threshold on oxygen concentration for [O]=0–42 at. %. The decrease of I_{thr} is approximately linear with the oxygen content. The melting threshold of 80 mJ/cm^2 for amorphous silicon is reduced to only half the value for the highest [O]. Since the substrate (Corning glass 7059) was identical for all samples, the observed behavior must be connected with the

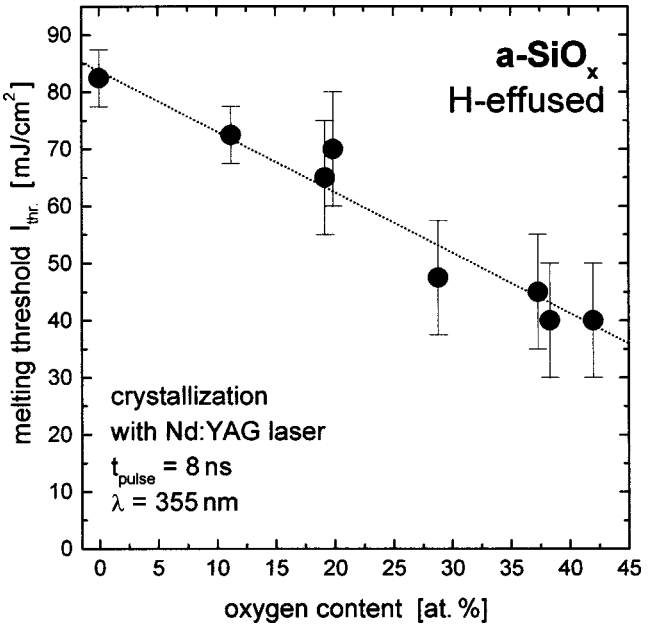

FIG. 3. Melting threshold I_{thr} of a-SiO_x upon laser pulse irradiation ($\lambda=355$ nm, $t_{pulse}=8$ ns) as a function of the oxygen content. The line is a linear fit to the data.

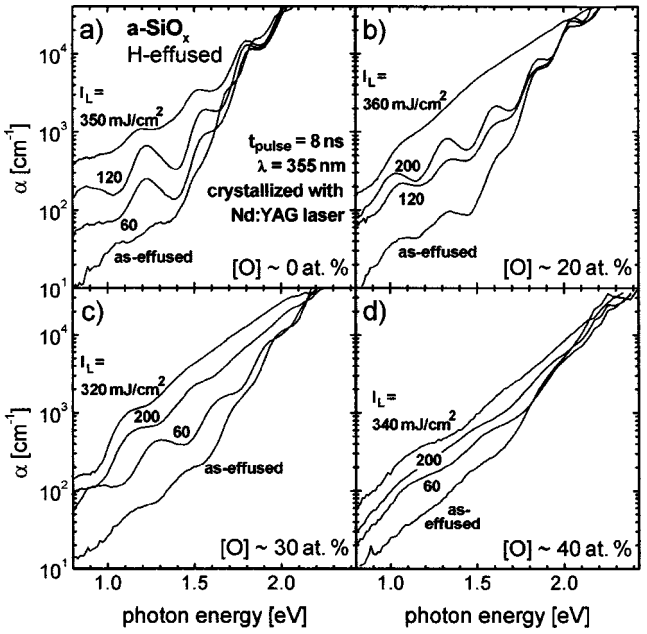

FIG. 4. Absorption spectra of H-effused a-SiO_x with [O]=0, 20, 30, and 40 at. %. The samples were irradiated with a single pulse at laser energy densities between 0 and 350 mJ/cm^2 ($\lambda=355$ nm, $t_{pulse}=8$ ns).

characteristics of the SiO_x films themselves. Over the range of oxygen concentrations studied, the material properties gradually change from those of silicon towards those of silicon dioxide. The thermal conductivities of pure a-Si ($\approx 5\ W\,m^{-1}\,K^{-1}$)[28,29] and a-SiO_2 ($1.38\ W\,m^{-1}\,K^{-1}$)[30] differ by a factor of about 4 at room temperature, whereas the heat capacities of a-Si and a-SiO_x are almost identical ($\approx 0.7\ kJ\,kg^{-1}\,K^{-1}$). Thus, we can assume that the reduction of the melting threshold arises from the decreasing thermal conductivity of the silicon suboxide layers with increasing oxygen concentrations. The heat generated at the film surface due to the absorption of the laser pulse can no longer be dissipated so rapidly to the substrate. The ensuing heat pileup will cause a melting of the film surface at smaller laser energy densities.

B. Changes of optical properties

The knowledge of the individual melting threshold allows a comparison of the laser crystallization process in different silicon suboxides. In Fig. 4 the optical absorption spectra of four different silicon suboxides (0, 20, 30, and 40 at. % [O]) are shown. They were irradiated homogeneously with single laser pulses up to 350 mJ/cm^2, which is far above the melting threshold of all samples. The as-effused a-SiO_x samples (1 h at 450 °C) exhibit properties which correspond to those in Fig. 1(b). In this state, a distinction between the band tail and the defect absorption is still possible for all oxygen concentrations. Upon laser irradiation, a strong broadening of the band tails occurs [Figs. 4(a)–4(c)]. Also the position of the optical gap E_{04} is shifted to smaller energies, however, not due to a shift of the band edges themselves but because of the influence of additional band tail states at $\alpha=10^4\ cm^{-1}$. In the region of defect absorption, a strong increase of the absorption coefficient is observed, as well, which makes a distinction between band tail and defect states difficult. This rise comprises almost 2 orders of magnitude for oxygen concentrations up to 30 at. % [Figs. 4(a)–4(c)] but becomes weaker for the sample with 40 at. % [Fig. 4(d)] where it is only a factor of about 10. Also the band tail broadening is less pronounced for [O]=40 at. %.

Moreover, an additional absorption shoulder at 1.1–1.2 eV, the energy of the indirect band gap of crystalline silicon, seems to emerge after illumination with high pulse energy densities. (This feature in the laser-irradiated absorption spectra should not be confused with the defect absorption shoulder of as-effused amorphous samples which appears at considerably smaller values of α and is additionally disturbed by strong thin film interference fringes.) Such a shoulder at 1.2 eV is best visible for the highest I_L in Figs. 4(b) and 4(c) where the absorption spectra are much less disturbed by interference fringes than for some of the smaller laser pulse energies. Despite some remaining uncertainty due to interferences this can be interpreted as a first indication for a laser-induced phase separation into silicon crystallites and the remaining amorphous SiO_x matrix, a behavior which is also suggested by the binary Si–O phase diagram.[31]

Also the weaker increase of the subgap absorption for larger oxygen contents ([O]$\geqslant$40 at. %) can be understood: The decreasing fraction of silicon limits the formation of large numbers of crystallites. Furthermore, the liquidus curve in the binary Si–O phase diagram increases from $T=1350$ to 1700 °C for [O]=25–50 at. %. As a consequence, resolidification tends to take place already at higher temperatures for larger oxygen contents and limits the time available for the occurrence of a phase separation. However, for laser energy densities far above the melting threshold which produce temperatures considerably larger than those discussed in connection with the liquidus curve, this effect is likely to be only of

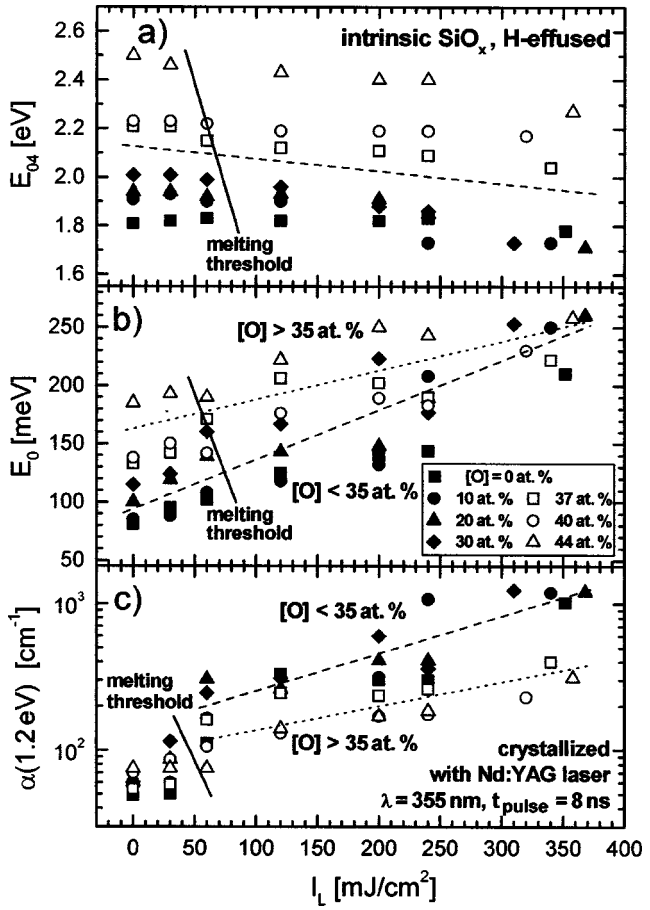

FIG. 5. Optical band gap E_{04} (a), Urbach energy E_0 (b), and subgap absorption α(1.2 eV) (c) of H-effused, laser irradiated a-SiO_x samples ([O]=0–44 at. %) as a function of the laser energy density I_L (λ=355 nm, t_{pulse} =8 ns). The lines are guides to the eye.

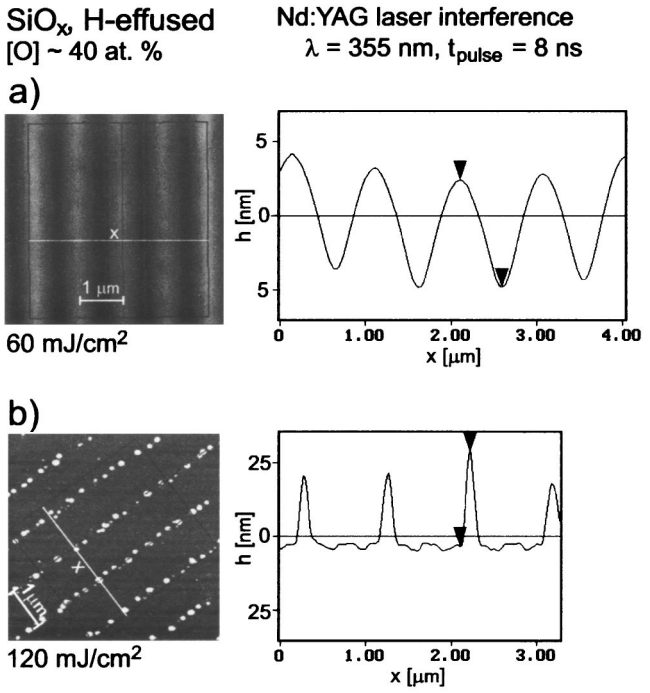

FIG. 6. Atomic force micrographs and cross sections of a-SiO_x with 40 at. % oxygen, crystallized by means of pulsed two-beam interference (λ =355 nm, t_{pulse}=8 ns) at average laser energy densities of 60 (a) and 120 mJ/cm^2 (b). The grating period was 1 μm.

minor influence. Additionally, more defects and disorder are initially present in samples with higher [O] so that laser irradiation is unable to further increase N_D or E_0 to such a great extent. Note that the term ''laser crystallization'' in the case of silicon suboxides can only be used within certain limits, since the formation of crystallized regions tends to become more unlikely or even impossible for higher [O].

A detailed analysis of the absorption spectra of laser irradiated silicon suboxides [cf. Fig. 4] with respect to the optical band gap, the Urbach energy, and the absorption at 1.2 eV is given in Figs. 5(a)–5(c) for oxygen concentrations between 0 and 44 at. %. The melting threshold is marked by a solid line in all graphs. As indicated by the dashed line in Fig. 5(a), the band gap E_{04} of all samples decreases in a similar way as a function of I_L. This is due to the overlap of additional band tail states produced by the laser pulses, which can also be seen from the behavior of the Urbach energy [Fig. 5(b)]. Here, E_0 strongly increases with laser energy density. However, the rise is more pronounced for samples with oxygen contents up to 30 at. % (solid symbols) than for silicon suboxides with 40 at. % oxygen or more (open symbols). For the highest $I_L \approx 350\,\mathrm{mJ/cm^2}$, all Urbach energies reach similar values above 200 meV, irrespective of [O]. A similar behavior of E_0 has also been observed for a-SiO_x:H samples which were implanted by high energy Er^{3+} ions (100–400 keV).[32]

The absorption coefficient at 1.2 eV [corrected for the disturbing influence of interference fringes, Fig. 5(c)] can be regarded as an approximate measure for the concentration of silicon crystallites embedded in the amorphous suboxide matrix after the incidence of the laser pulse. Below the melting threshold, α(1.2 eV) exhibits comparable values for all oxygen concentrations, caused by the higher defect density in hydrogen effused samples. Above I_{thr}, however, obvious differences exist for samples below and above 35 at. % [O]. Up to 30 at. %, the absorption at 1.2 eV is significantly larger than for samples with higher amounts of oxygen. This difference comprises about 1/2 order of magnitude at the maximum energy densities applied. From these results it can be concluded that the susceptibility for the formation of Si crystallites is high and approximately constant for smaller oxygen contents ([O]<35 at. %), whereas for larger [O] such a crystallization process seems to become less likely. This conclusion is also corroborated by the structural investigations described below.

C. Structural changes upon laser irradiation

In order to shed more light on the nature of the structural modifications which are caused by the laser irradiation, an analysis of the sample surfaces was performed by AFM. Figure 6 shows AFM micrographs of a sample with 40 at. % oxygen which was irradiated by means of two-beam interference. This resulted in an intensity line grating with 1 μm period. Note that due to the modulated intensity profile, the average laser energy densities applied here (60 and 120

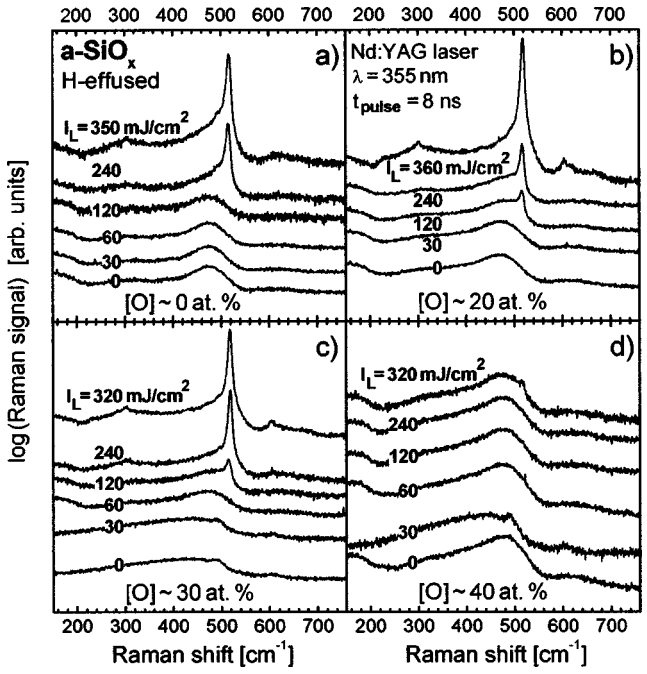

FIG. 7. Raman spectra of silicon suboxides with 0, 20, 30, and 40 at. % oxygen, irradiated with single Nd:YAG laser pulses ($\lambda = 355$ nm, $t_{\text{pulse}} = 8$ ns) up to $I_L \approx 350$ mJ/cm^2. Note the logarithmic intensity scale!

mJ/cm^2) cannot be compared directly to similar values of I_L in experiments with homogeneous illumination, but are both clearly above the melting threshold in the regions of constructive interference. Also, the sample examined has a large oxygen content (40 at. %), for which only a reduced number of crystalline inclusions is expected to form.

The laser energy density of 60 mJ/cm^2 [Fig. 6(a)] leads to a smooth periodic patterning of the suboxide with an amplitude below 10 nm. In contrast, for $I_L = 120$ mJ/cm^2 [Fig. 6(b)], well-separated sharp spots become visible along the lines of maximum intensity. Their height is as large as 25 nm. Similar pileup effects are known to also occur along the center of interference maxima for pure *a*-Si, however, not in the shape of such pronounced spots but rather as continuous linear features.[15,17,33] A partial ablation or evaporation of the layer can be excluded since these processes take place at considerably larger pulse energies. The results shown in Fig. 6(b) are not yet proof of a phase separation in SiO_x, but clearly indicate the occurrence of structural inhomogeneities upon laser irradiation. Note that it was concluded from Fig. 5 that *a*-SiO_x with oxygen contents exceeding 35 at. % did not show a tendency for Si-crystallite formation in the case of homogeneous laser irradiation. However, laser interference irradiation gives rise to higher peak intensities and to additional lateral thermal gradients, which apparently can also stimulate crystallite formation in the case of high oxygen concentrations.

Definitive evidence for the formation of silicon crystallites by phase separation was obtained by Raman spectroscopy. Figure 7 shows (on a logarithmic scale) Raman spectra for four different SiO_x samples (0, 20, 30, and 40 at. % [O]) which were irradiated with laser energy densities up to 350 mJ/cm^2. In the spectrum of the H-effused *a*-Si sample [Fig. 7(a)], the characteristic peak of amorphous silicon at 480 cm^{-1} is dominant at low pulse energies. For $I_L > 120$ mJ/cm^2, the typical signal of crystalline silicon becomes visible as a sharp peak at about 520 cm^{-1},[1] which is the expected behavior for laser crystallized pure amorphous silicon. For the highest laser energies, second order Raman scattering can also be identified as a small feature around 300 cm^{-1}, whereas the amorphous peak has almost completely vanished. A similar behavior is observed for the suboxide samples with 20 and 30 at. % oxygen [Figs. 7(b) and 7(c)]. Again, for $I_L \gtrsim 120$ mJ/cm^2, an intense *c*-Si Raman peak prevails in the spectra and confirms the existence of a phase separation and the formation of Si crystallites in the amorphous SiO_x matrix. Due to the reduced melting threshold of these samples, crystallites already form at lower I_L compared to the case of pure *a*-Si. The thresholds for surface melting (cf. Figs. 2 and 3) and for crystallite formation are not identical, though. This can be seen as an indication that a crystallization of the material can only take place after a sufficiently large volume fraction is liquified for a sufficiently long time.

For the sample with 40 at. % [Fig. 7(d)], however, the situation is different. Here the amorphous peak ($\nu = 480$ cm^{-1}) persists in the spectra for all irradiation intensities and only a tiny crystalline signal emerges at the highest I_L. This observation nicely confirms the conclusions from Figs. 4, 5, and 6 that the formation of crystalline domains is increasingly suppressed for oxygen contents larger than 40 at. %. The small feature noticeable in some of the spectra at 490–500 cm^{-1}, even before laser irradiation, is not due to Si crystallites, but probably arises from already existing SiO_2 clusters in the samples or from the Corning glass substrate which exhibits a broad peak at these wave numbers.

For a more quantitative analysis of the crystallite formation in silicon suboxides, Fig. 8 displays the Raman spectra of samples with [O]=0–44 at. %. They were irradiated by a single laser shot with an energy density of 350 mJ/cm^2, i.e., far above the respective melting thresholds. From the logarithmic plot in Fig. 8(a) it is clear that samples up to 30 at. % oxygen can be crystallized very efficiently and almost independently of the oxygen content. The *c*-Si peak is significantly reduced for 37 at. % [O], nearly disappears for 40 at. % and no longer exists for even larger [O]. Thus, the oxygen threshold concentration for a phase separation of silicon suboxides upon intense pulsed laser irradiation can be determined to be [O]=40 at. % for intensities up to 350 mJ/cm^2. At even higher pulse energies, partial evaporation of the samples occurs.

The plot of the *c*-Si peaks on a linear scale in Fig. 8(b) permits a quantitative comparison of the SiO_x crystallization process below [O]=40 at. %. The largest signal intensities, corresponding to the best crystalline quality or largest grain sizes, can be observed for moderate oxygen contents between 10 and 30 at. %. As a matter of fact, the intensity of the 520 cm^{-1} signal is considerably larger for *a*-SiO_x than for pure amorphous silicon.

A quantitative line shape analysis of the *c*-Si peaks of Fig. 8(b) is shown in Fig. 9. The enhanced quality of crystals in silicon suboxides with [O]=10–30 at. % is confirmed not

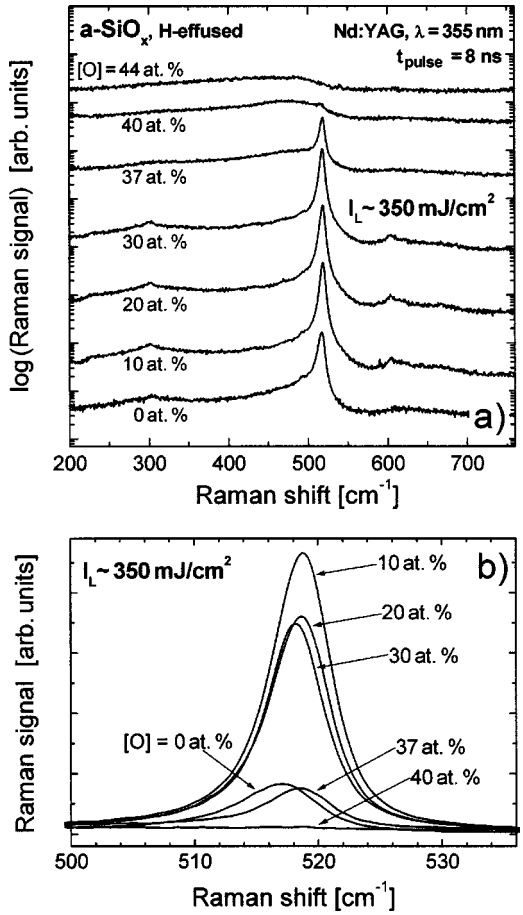

FIG. 8. Raman spectra of SiO_x with [O]=0–44 at. % after irradiation with a single ND:YAG laser pulse (λ=355 nm, t_{pulse}=8 ns) of $I_L \approx 350\ mJ/cm^2$: (a) logarithmic plot and (b) enlarged view of the 520 cm^{-1} peak on a linear scale.

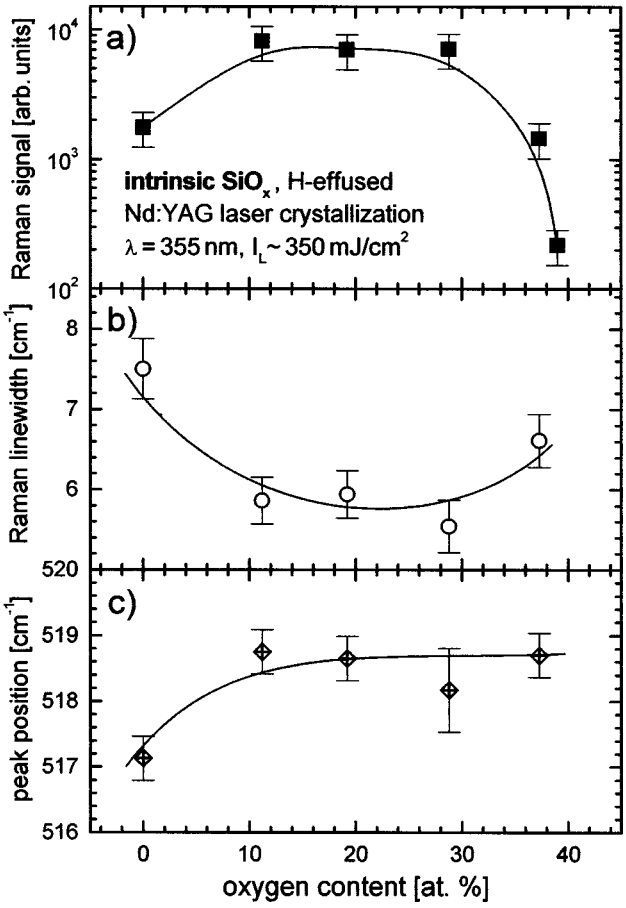

FIG. 9. Intensity (a), linewidth (b), and position (c) of the crystalline Si Raman peak of crystallized SiO_x as a function of the oxygen concentration ($I_L \approx 350\ mJ/cm^2$, λ=355 nm, t_{pulse}=8 ns).

only by the signal intensity but also by the behavior of the linewidth and position of the *c*-Si peak. The Raman intensity [Fig. 9(a)] is a factor of 4–5 higher for SiO_x with moderate oxygen fractions compared to crystallized amorphous silicon alone. Also, the oxygen threshold concentration of 40 at. % is clearly visible as a decrease of the signal by almost 2 orders of magnitude. A noticeably larger crystallite size is suggested by the decrease of the Raman linewidth $\Delta\nu$ in Fig. 9(b). $\Delta\nu$ is reduced from a value of 7.5 cm^{-1} for [O]=0 at. % to around 6 cm^{-1} for [O]=10–30 at. % and increases only slightly again for the sample with 37 at. % oxygen. Also the peak position [Fig. 9(c)] is shifted from ν=517 cm^{-1} (0 at. % [O]) towards ≈519 cm^{-1} and thus approaches the value of 520 cm^{-1} for bulk *c*-Si.

By means of TEM the size, distribution, and orientation of the Si crystallites in *a*-SiO_x as well as the thickness of the crystallized layers can be determined. Among the silicon suboxides crystallized with $I_L = 350\ mJ/cm^2$ (cf. Figs. 8 and 9), the samples with 0 and 30 at. % oxygen were selected for cross section TEM analysis.

Figure 10(a) shows the dark field image from the 111 reflection for the H-effused *a*-Si sample. Three regions corresponding to the glass substrate, the remaining noncrystallized *a*-Si(≈230 nm), and the laser-crystallized μc-Si (≈200 nm) can be distinguished. The microcrystalline layer exhibits a columnar structure perpendicular to the surface and some larger Si crystallites at the surface with dimensions up to 50 nm can be recognized. The nonperiodic interference lines which characterize some of the crystalline formations indicate the existence of twin crystals. The diffraction pattern [inset of Fig. 10(a)] shows rather sharp rings which demonstrate the high crystallinity and the statistical orientation of the Si crystallites. However, slightly defocused bright field micrographs (not shown) suggest that the Si crystallites are still separated by small voids or thin amorphous intermediate layers.

The dark field micrograph of the silicon suboxide sample with 30 at. % oxygen [Fig. 10(b)] also shows the substrate, the noncrystallized SiO_x(≈290 nm), and a microcrystalline surface layer produced by laser irradiation ($I_L = 350\ mJ/cm^2$). In contrast to pure amorphous silicon, no depth homogeneity exists in the microcrystalline region and there are no indications for columnar growth. Several crystallites as large as 200 nm are present at the surface, whereas underneath small grains (<20 nm) are homogeneously distributed. The surface is rough and its topology is determined by the spherical shape of the large surface crystallites [Fig. 10(b)]. They are surrounded by a bright diffuse band which might be an indication for coverage by a (possibly O-rich) amorphous phase. Also, intermediate voids of up to 30 nm are likely to exist in the region of the large crystallites. The

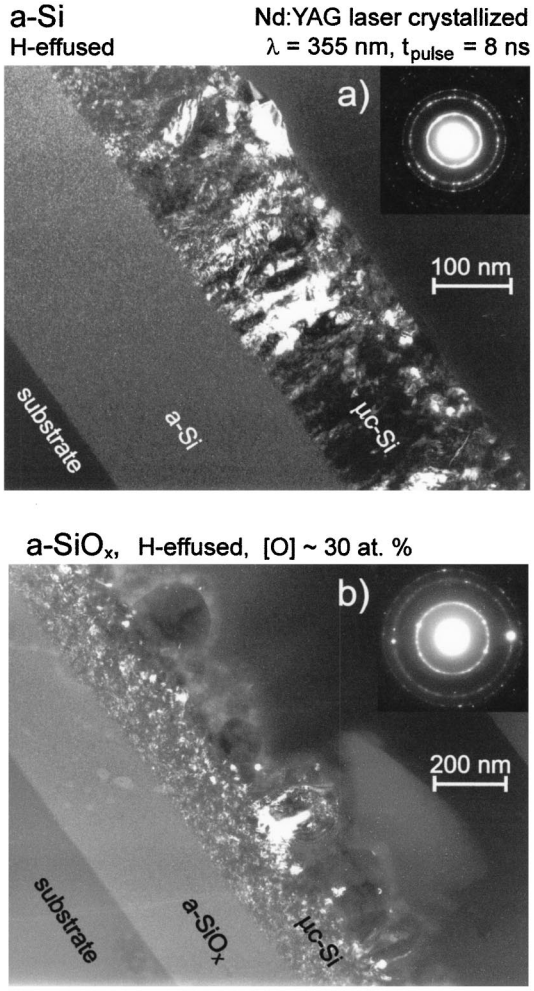

FIG. 10. Transmission electron micrographs of cross-sectional samples of a-Si (a) and a-SiO_x:H with 30 at. % oxygen (b) crystallized with single Nd:YAG laser pulses of $I_L = 350\ mJ/cm^2$ ($\lambda = 355$ nm, $t_{pulse} = 8$ ns). The insets show the corresponding diffraction patterns.

diffraction pattern [inset of Fig. 10(b)] confirms the random orientation of the crystallites in the small grain layer. Some strong distinct diffraction maxima arising from the large surface crystals are also present.

An important aspect of laser crystallization in amorphous Si-based materials deserves some more attention: Crystal formation and phase separation processes do not only take place in the liquified Si/SiO_x mixture. Solid phase crystallization also occurs in the unmolten part of the samples starting from the liquid/solid interface towards the substrate. These two crystallization regimes have to be regarded separately. For pure silicon [cf. Fig. 10(a)] the region of solid phase crystallization (in the vicinity of the unmolten a-Si) is characterized by a columnar structure, whereas liquid phase crystallization results in some isolated larger crystals ($\approx$50 nm) close to the surface. Also for the SiO_x sample with 30 at. % oxygen the two different regimes can be distinguished: large crystallites ($\approx$200 nm) at the surface and small grains underneath ($\approx$20 nm). Assuming that a phase separation in the suboxide also occurs in the region of solid phase crystallization, the small silicon crystals are likely to be separated from each other by the remaining suboxide matrix. Thus, the lack of a columnar growth structure in Fig. 10(b) could be understood. A more detailed analysis, in particular with respect to the nature of the remaining amorphous SiO_x material between or around the Si crystallites, is not possible from the present data. Nevertheless, the regions of liquid and solid phase crystallization can be identified both for the a-Si and the a-SiO_x sample. Moreover, there exist indications that a phase separation, though of different character, occurs for both regimes in the suboxide with 30 at. % oxygen.

In summary, the findings from Raman spectroscopy are confirmed: in laser irradiated SiO_x samples with [O]=10–30 at. % larger Si crystallites ($\approx$200 nm) are formed compared to pure amorphous silicon ($\approx$50 nm). Generally, the largest grains in a-Si are known to grow in a narrow intermediate regime of laser energy densities, the so called SLG regime.[11–15] The enlarged crystallites observed for silicon suboxides with moderate oxygen concentrations indicate that the presence of oxygen helps to achieve a similar favorable growth regime. The reduced thermal conductivity of the SiO_x films results in a heat pileup after the laser pulse which prolongs the resolidification process and promotes larger grain sizes. However, the role of the oxygen atoms and the details of the phase separation also have to be taken into account for a profound understanding of laser crystallization in a-SiO_x.

V. CONCLUSIONS

H-effused silicon suboxides with 0–44 at. % oxygen were subjected to intense Nd:YAG laser pulses in order to study crystallization and phase separation as a function of the oxygen concentration. The surface melting threshold of the different samples was found to decrease linearly with [O] from above 80 mJ/cm^2 for a-Si to approximately 40 mJ/cm^2 for oxygen contents above 40 at. %. Based on optical absorption measurements and Raman investigations, it was demonstrated that for silicon suboxides with oxygen concentrations below 40 at. % a phase separation in Si crystallites and in a surrounding SiO_x matrix occurs upon laser irradiation. This was further corroborated by TEM measurements and atomic force micrographs. Laser irradiated silicon suboxides with oxygen contents between 10 and 30 at. % exhibit a large signal of the c-Si Raman peak ($\nu \approx 520\ cm^{-1}$), which is even significantly stronger than that of pure recrystallized a-Si. Also the Raman linewidth and the peak position suggest that for moderate oxygen contents silicon crystals with enhanced quality and larger grain size are formed. TEM micrographs gave evidence that in this favorable range of oxygen concentrations ([O]=10–30 at. %), the dimension of the largest Si crystallites is approximately 200 nm, whereas for a-Si alone the maximum grain size is limited to 50 nm. However, above an oxygen threshold concentration of 40 at. %, no Si crystallites could be produced by means of laser pulses with energy densities up to 350 mJ/cm^2. Apparently, the increasing oxygen content in the samples prevents an efficient formation of nc-Si or μc-Si inclusions.

ACKNOWLEDGMENT

This work was supported by the Deutsche Forschungsgemeinschaft (DFG Project No. Stu. 139/6-3).

[1] M. Stutzmann, in *Handbook on Semiconductors*, edited by T. S. Moss and S. Mahajan (Elsevier Science B. V., Amsterdam, 1994), Vol. 3, p. 657.
[2] M. Stutzmann, W. B. Jackson, and C. C. Tsai, Phys. Rev. B **32**, 23 (1985), and refs. therein.
[3] H. M. Branz, Sol. Energy Mater. Sol. Cells **78**, 425 (2003), and references therein.
[4] D. E. Carlson, Sol. Energy Mater. **8**, 129 (1982).
[5] J. I. Pankove, Sol. Energy Mater. **8**, 141 (1982).
[6] C. R. Wronski, in *Semiconductors and Semimetals*, edited by J. I. Pankove (Academic, New York, 1984), Vol. 21C, p. 347.
[7] W. Fuhs, H. Mell, J. Stuke, P. Thomas, and G. Weiser, Ann. Phys. (Leipzig) **42**, 187 (1985).
[8] M. Stutzmann and C. E. Nebel, Encycl. Appl. Phys. **18**, 151 (1997).
[9] R. A. Lemons, M. A. Bosch, A. H. Dayem, J. K. Grogan, and P. M. Makiewich, Appl. Phys. Lett. **40**, 469 (1982).
[10] G. Andrä, J. Bergmann, F. Falk, E. Ose, and H. Stafast, Phys. Status Solidi A **166**, 629 (1998).
[11] J. S. Im, H. J. Kim, and M. O. Thompson, Appl. Phys. Lett. **63**, 1969 (1993).
[12] J. S. Im, M. A. Crowder, R. S. Sposili, J. P. Leonard, H. J. Kim, J. H. Yoon, V. V. Gupta, H. J. Song, and H. S. Cho, Phys. Status Solidi A **166**, 603 (1998).
[13] J. B. Boyce, P. Mei, R. T. Fulks, and J. Ho, Phys. Status Solidi A **166**, 729 (1998).
[14] G. Aichmayr, D. Toet, M. Mulato, P. V. Santos, A. Spangenberg, S. Christiansen, M. Albrecht, and H. P. Strunk, Phys. Status Solidi A **166**, 659 (1998).
[15] G. Aichmayr, D. Toet, M. Mulato, P. V. Santos, A. Spangenberg, S. Christiansen, M. Albrecht, and H. P. Strunk, J. Appl. Phys. **85**, 4010 (1999).
[16] C. E. Nebel, S. Schöniger, B. Dahlheimer, and M. Stutzmann, Mater. Res. Soc. Symp. Proc. **467**, 421 (1997).
[17] C. Eisele, in *Selected Topics of Semiconductor Physics and Technology* Vol. 47, edited by G. Abstreiter, M. C. Amann, M. Stutzmann, and P. Vogl (Walther Schottky Institute, Munich, 2000).
[18] R. Janssen, in *Selected Topics of Semiconductor Physics and Technology* Vol. 31, edited by G. Abstreiter, M. C. Amann, M. Stutzmann, and P. Vogl (Walther Schottky Institute, Munich, 2000).
[19] W. B. Jackson, N. M. Amer, A. C. Boccara, and D. Fournier, Appl. Opt. **20**, 1333 (1981).
[20] D. A. Papaconstantopoulos and E. N. Economou, Phys. Rev. B **24**, 7233 (1981).
[21] B. von Roedern, L. Ley, and M. Cardona, Phys. Rev. Lett. **39**, 1576 (1977).
[22] B. von Roedern, L. Ley, and F. W. Smith, in *The Physics of Semiconductors*, edited by L. H. Wilson (Institute of Physics, London, 1978), p. 701.
[23] B. von Roedern, L. Ley, M. Cardona, and F. W. Smith, Philos. Mag. B **40**, 433 (1979).
[24] D. C. Allan, J. D. Joannopoulos, and W. B. Pollard, Phys. Rev. B **25**, 1065 (1982).
[25] D. C. Allan, J. D. Joannopoulos, and W. B. Pollard, Phys. Rev. B **26**, 3475 (1982).
[26] E. C. Freeman and W. Paul, Phys. Rev. B **20**, 716 (1979).
[27] T. D. Moustakas, in *Semiconductors and Semimetals*, edited by J. I. Pankove (Academic, Orlando, 1984), Vol. 21A, p. 55.
[28] L. Wei, M. Vaudin, C. S. Hwang, and G. White, J. Mater. Res. **10**, 1889 (1995).
[29] S. Uma, A. D. McConnell, M. Asheghi, K. Kurabayashi, and K. E. Goodson, Int. J. Thermophys. **22**, 605 (2001).
[30] Heraeus Quarzglas GmbH & Co.KG, in *Quarzglas für Die Optik, Daten und Eigenschaften* (Hanau, 1999).
[31] *Binary Alloy Phase Diagrams*, edited by Th. B. Massalski (American Society for Metals, Metals Park, OH, 1986).
[32] A. Janotta, M. Schmidt, R. Janssen, Ch. Buchal, and M. Stutzmann, Phys. Rev. B **68**, 165207 (2003).
[33] D. K. Fork, G. B. Anderson, J. B. Boyce, R. I. Johnson, and P. Mei, Appl. Phys. Lett. **68**, 2138 (1996).